The 2009 IEEE/RSJ International Conference on
Intelligent Robots and Systems
October 11-15, 2009 St. Louis, USA

Parasitic Effects on Nanoassembly Processes

Thomas Wich, Christian Stolle, Christoph Edeler and Sergej Fatikow

Abstract— **This paper analyzes the disturbance sources acting on nano-assembly systems inside the scanning electron microscope, which complicate the automation of assembly processes in the scanning electron microscope. The influence of intrinsic sources, i.e. thermal drift, actuator offset and end effector vibrations due to actuator movements are examined and approaches are suggested. The electron-beam interaction with the assembly system has been identified as another disturbance source and its impact on automated assembly processes is qualified and quantified. Solutions for disturbance-resistant assembly processes are suggested.**

I. INTRODUCTION

When Eigler et al. demonstrated the manipulation of atoms using the tip of a scanning tunneling microscope (STM) in 1989 [1], the nano-scale manipulation became of interest to the research community. In the beginning of the 1990's, manipulation of micro- and nano-scale objects evolved as a major research topic, mainly driven by Japanese research institutes [2], [3], [4]. The basic motivation at that time was the industry-driven necessity to characterize integrated circuits, measure surface characteristics of storage media, mechanical characterization of thin films [2] and the common trend towards miniaturization [4]. Many of these experiments have been performed in the scanning electron microscope (SEM), which is used widely due to its high resolution in the nm-range and comparatively short image acquisition time.

Today, the challenge is not only to handle, manipulate or assemble parts in the SEM, but to use this instrument for automated assembly [5], [6]. Under this aspect, many techniques have been developed which enable sophisticated position control for the end effectors, e.g. high precision drives utilizing stick-slip, noise-tolerant image processing algorithms [7] and visual servoing [8], [9].

In our experiments regarding automated assembly in the SEM we found many disturbance factors acting on the manufacturing process, which limit the capabilities of this interesting technique. Therefore, we analyzed typical disturbance sources within this paper in order to qualify and quantify their impact on the process and to lay the foundation for improving the automated assembly process.

As a starting point, the setup of the assembly system will be described in section II. The disturbance sources are divided in three major categories. In section III, the disturbances coming from the assembly system itself, i.e. the actuators and sensors, are analyzed. Afterwards, the interactions between the SEM's electron beam and the assembly system are examined in section IV. The third category, extrinsic sources (acoustic noise and building vibrations), will not be discussed here.

Division Microrobotics and Control Engineering, Department of Computing Science, University of Oldenburg, 26111 Oldenburg, Germany stolle@informatik.uni-oldenburg.de

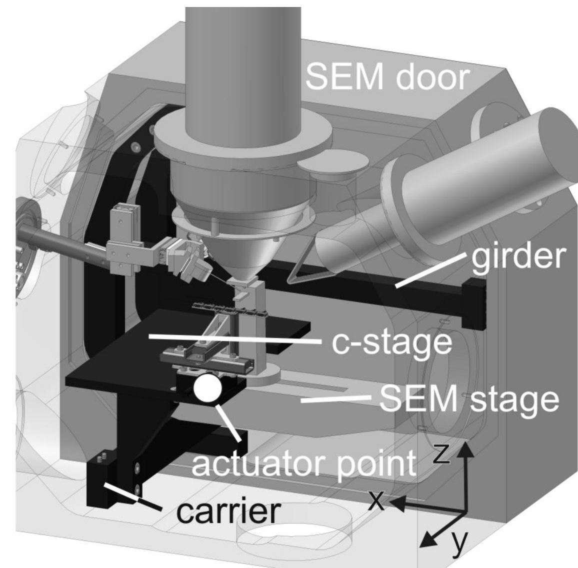

Fig. 1. Drawing of the experimental setup (for details see Section II).

II. EXPERIMENTAL SETUP

Two cartesian X-Y-Z stages with coarse and fine positioning capabilities are needed for the cantilevers and for the touchdown alignment. The stage coming with the SEM (SEM-stage) positions the touchdown sensor, providing a sufficient positioning accuracy of 1 μm. Thus, the aim of this setup is to integrate an additional stage (c-stage) including positioners to the SEM chamber, as shown in Fig. 1. For fine positioning of the cantilevers in relation to the touchdown sensor three linear axes (X, Y, Z, SmarAct GmbH) and a linear axis (Z, Physik Instrumente GmbH) were chosen. The latter, to enable single nanometer accuracy with sensor feedback. These four actuators are combined to the c-stage. A mechanical link to the SEM is designed, which leads to the actual setup, black parts represent the c-stage. The actuators are mounted to the upper part of the c-stage, which is hold in position by a carrier at the bottom and a girder. All parts are made of aluminum (AW-2017), the surface was finished by sandblasting and acid.

Several constraints determined the design of the c-stage. First of all, the SEM should not be modified, the possibility to remove the stage should be kept. This leads to a clamp-mechanism, which holds the c-stage inside the SEM chamber. Secondly, the c-stage with the actuators needs to

TABLE I

LIST OF RELEVANT EIGENMODES OF THE C-STAGE

Mode	Freq. [Hz]	Direction	Type
1	198	X	Bend of baseplate and carrier
2	270	Z	Bend of baseplate and carrier
3	382	Z	Torsion of baseplate
4	473	Z	Bend of baseplate
5	654	-	Bend of carrier
6	942	Z	Partial baseplate bend
7	1021	-	Bend of baseplate

be easily accessible. This is reached by attaching the clamp-mechanism to the SEM-door. By opening the door, the entire c-stage is pulled out of the chamber. The most important constraint is to avoid possible collisions with the sensitive SEM-detectors, but enabling the positioning capabilities of the SEM-stage. Especially the internal homing of the SEM-stage must not be hindered, because it is essential for automation. However, keeping the full function of the SEM-stage featuring five degrees of freedom (DoF) is impossible due to the large clearance. Thus, a trade-off has to be found. We decided to restrict the Z-travel to 10 mm and to skip the tilt-DoF. This leads to the presented setup.

Table I shows the results of a finite element (FE) eigenfrequency analysis of the c-stage. The weight of the actuators is estimated to be 170 g and is represented by an additional mass in the FE-model. The eigenmodes were categorized by the type of motion of the point, where the actuators are mounted to the base plate (see Fig. 1, actuator point). The entry "direction" in Table I indicates the particular impact to the actuators. The most important eigenmodes with relevance to the actuators are 1, 2, 3, 4 and 6. Thus, the corresponding frequencies should be avoided by any actuator. Eigenmodes 5, 7 and eigenfrequencies higher than 1.1 kHz are of minor relevance, either because of the movement type or to the small amplitudes.

III. INTRINSIC SOURCES

A. Thermal Drift Due to Dissipation Loss

Thermal expansion is of essential importance for any system on the nano-scale, as typical thermal expansion coefficients are in the range of several $\mu\mathrm{m}/(\mathrm{m}\cdot\mathrm{K})$ while the geometrical size of sensors and actuators applied are still in the range of mm to cm. Typical sources for thermal dissipation loss are the drives within the actuators or the integrated sensors. In the SEM's vacuum chamber, heat dissipation is strongly limited due to missing convection. The convection usually contributes massively to the overall heat dissipation. Additionally, heat radiation is also neglected due to the low temperature and the small surface of typical assembly systems. Therefore, the main contribution for heat dissipation is based on heat conduction. Consequently, the warming of the system due to a heat source with power P, which is connected over a thermal resistor with heat conductivity λ, length δ and cross section A to a thermal reservoir with constant temperature can then be calculated to:

$$P = c_v \cdot m \cdot \frac{d\Delta T}{dt} + \frac{\lambda \cdot A}{\delta} \cdot \Delta T, \tag{1}$$

assuming a one dimensional problem. The parameter c_v is the specific thermal capacity and m the mass of the object. In Fig. 2, a typical example for an actuator with integrated sensor is shown. Based on the assumption, that the slip-stick drive can hold its position power-free, the only heat source is the position sensor, for which a thermal power of $P = 0.5\,\mathrm{W}$ is assumed [10].

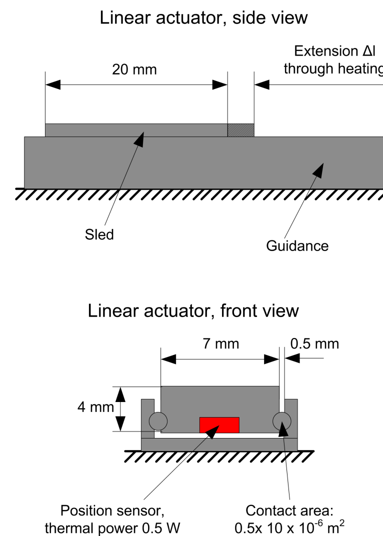

Fig. 2. Schematic view of the system assumed for estimating the thermal drift within actuators due to thermal power losses.

The steel-made sled ($\lambda = 14\,\mathrm{W}/(\mathrm{m}\cdot\mathrm{K})$, $c_V = 510\,\mathrm{J}/(\mathrm{kg}\cdot\mathrm{K})$, $m = 4.42\,\mathrm{g}$, $l = 20\,\mathrm{mm}$) heats under these conditions up by a temperature difference of 1.6 K after 10 s and approaching a value of $\Delta T = 3.6\,\mathrm{K}$ for $t = \infty$. Assuming a thermal elongation coefficient for steel of $k = 14\,\mu\mathrm{m}/(\mathrm{m}\cdot\mathrm{K})$, the elongation Δl of the sled and thus the, travel of the end effector can be calculated by:

$$\Delta l = l \cdot k \cdot \Delta T. \tag{2}$$

This results in elongations $\Delta l = 0.53\,\mu\mathrm{m}$ at $t = 10\,\mathrm{s}$ and $\Delta l = 1.14\,\mu\mathrm{m}$ for $t = \infty$.

The theoretic examples above show clearly, how dramatic the influence of heating for assembly processes on the micro- and nano-scale is. Not only the heating leads to a movement of the end effector, but the drift cannot be measured and controlled by the on-board sensors. Therefore, we suggest the following countermeasures:

- Minimizing of thermal power loss through using efficient actuators, preferably with no power consumption when holding a position, e.g. slip-stick actuators.
- Minimizing of thermal power loss of the sensor. Often, these sensors are built into the actuators constituting a heat source. These sensors should preferably be operated in a power-save modus while standing still.

- Applying sensors with little power insertion on the sled, e.g. laser interferometers instead of onboard sensors.
- Utilizing visual servoing [9], [8], [11] to control the end effector movement.

B. Misalignment Between Vision Plane and Actuator Coordinate System

Calibration of sensors and actuator systems leads to an important improvement in positioning accuracy. This is true in macrorobotics as well as microrobotics. The major differences of macro- and nanorobotics in the SEM are the long axis ranges compared to the accuracy demands, e.g. a few centimeters compared to several nanometer and the resulting long levers. Even small offset angles between two axes lead to a significant decrease of positioning accuracy of the whole system. For example an error angle of 0.1 degrees between two orthogonal central mounted cartesian axes of length 3 cm may lead to an end effector position error of 26 μm.

The position error of the c-stage in our experimental setup (cp. Section II) has been determined by moving each actuator axis separately $\pm 300\,\mu$m around the SEM image center at a magnification of 2000x. The travel distance has been determined by the internal axis sensors, which have an accuracy of several nanometers. The pixel displacement has been recorded and translated into meter. The results are $5.3\,\mu$m in x-direction and $2.92\,\mu$m in y-direction for a z-movement, $0.13\,\mu$m in x-direction for a y-movement and $2.19\,\mu$m in y-direction for an x-movement. Please note, that the z-displacement could not be determined due to the depth of focus of the SEM. The perspective influence of the projection (i.e. central perspective) is about $\pm 0.13\,\mu$m [12]. Therefore, the y axis is fairly well aligned with the image plane, while the others are not. For reliable positioning this displacement needs to be compensated for every movement.

C. End Effector Vibrations Through Actuator Movements

Vibrations through actuator movements are mainly generated by play of joints and guidance of axes as well as by the actuation principle. Especially the popular stick-slip drives introduce vibrations, which are transferred into the structure of the nanorobots. Small movements at the base of a robot have a huge impact on the end effector movements due to the long lever compared to the part and tool sizes. For low scan speeds the vibrations lead to staggered images of the end effector, which can lead to a loss of the tracked object. The higher the level of magnification, the higher the impact of the vibrations gets. Table II shows the impact of vibrations on the c-stage at different magnifications for a movement of 0.5 mm. The Settling time is the time required from reaching the end position until the vibration amplitude is below one pixel.

Counteractive measures are to increase the stiffness of the guidances and compact robots to decrease the joint play and to lower the lever. The automation sequences also need to compensate the vibrations by introducing settling times after actuator movements if visual feedback is required. For vibration sensitive tasks such as bringing tools and parts into contact, an additional axis with a continuous drive as for example a piezo stack can be very useful.

TABLE II

EFFECT OF A STICK-SLIP MOVEMENT OF 0.5 MM ON AN END EFFECTOR MOUNTED ON TOP OF THE C-STAGE.

Magnification	max. Amplitude [px]	Settling Time [s]
150	0.4	0.1
500	1.5	0.8
800	2.3	1.2
2000	10.6	2.1
4000	25.1	2.3

IV. E-BEAM INTERACTION BASED DISTURBANCES

The assembly system is set-up in the SEM, which is used for observing the assembly process. SEM images are generated by pinpointing the focused electron beam with a defined acceleration voltage U_A on the scene. The primary electrons of the beam interact with the objects within the scene in terms of emission of low-energy secondary electrons ($E_{SE} < 50\,\text{eV}$), high energetic backscattered electrons ($50\,\text{eV} < U_{BSE} < e \times U_E$) and the generation of e.g. X-rays. For imaging, usually the secondary electrons (SE) are collected by means of an Everhardt-Thornley-detector (ETD). By scanning the electron over the scene in x- and y-direction, the image is constructed. However, this image formation process can — especially in assembly systems — be disturbed by several effects, which will be explained in the next sections.

A. Shading

The generated low-energy SE are attracted by the Everhardt-Thornley detector by applying a suction voltage, usually in the range of 300 V. All other parts within the vacuum chamber are grounded to 0 V. The emitted SE leave the surface of the scanned objects and are then accelerated towards the ETD along the electric field trajectories.

While in analytical SEM's at least a quasi-static electric field can be assumed, the electric field in SEM's modified for assembly processes cannot be considered constant anymore. Although the moving parts of the assembly system, e.g. tools for handling, are grounded, the positioning of these tools leads to a change electric fields gradients. In Fig. 3, a simulation of the electric field lines inside the SEM-chamber is shown. All elements except the ET-detector are grounded. The embedded image shows a magnified view the assembly system.

Based on this scene, the influence of a grounded tool used for the manipulation of objects on the parts carrier has been simulated, in order to find out, how the image made from the scan field is influenced by the presence of such movable tools. As a measure, the electric field strength along the scan field has been selected. As a parameter, the distance between the incidence of the e-beam at $x = 0\,\text{mm}$ in the middle of the scan field and the tool tip has been used. In Fig. 4 the results are plotted, showing a strong influence of the tool on the electric field strength.

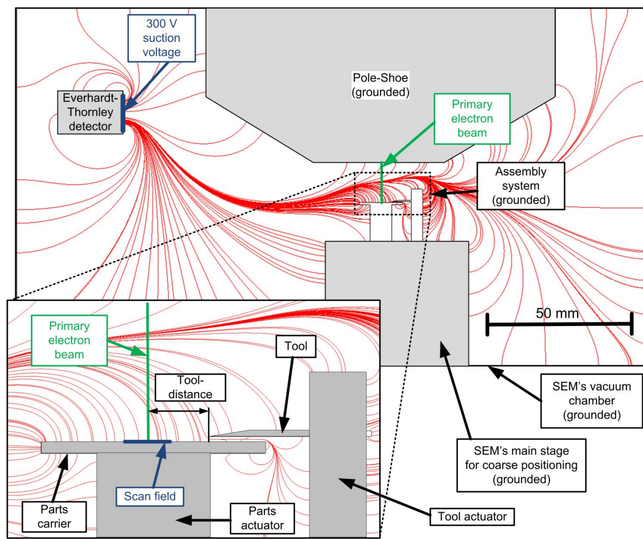

Fig. 3. Simulation of the electric field lines in the SEM-chamber with the assembly system.

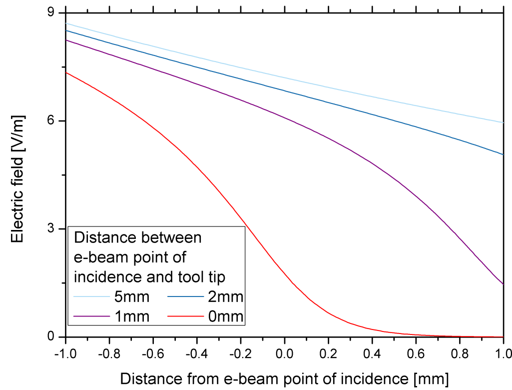

Fig. 4. Results of the simulation of the electric field strength along the scan field size (cp. Fig. 3). As a parameter, the distance between the e-beam incidence ($x = 0$mm) and the tool tip is used.

In fact, the approach of the tool towards the scan field leads to a strong deformation of the electric field. Consequently, the image quality will be strongly influenced in brightness and contrast, as the emission and acceleration of SE towards the ETD is affected. For automation of nano-assembly tasks based on object recognition and visual servoing it is thus necessary to either use algorithms which are resistant against changes in brightness and contrast, respectively, or to apply several image optimization steps (cp. Tab. III).

B. Charging Effects

Although every part of the assembly station should be grounded, charging cannot be prevented completely. There are two mechanisms which add to charging. The first effect is based on the balance between injected and emitted electrons. At high acceleration voltages less electrons are emitted than injected for certain materials (e.g. silicon) due to their low coefficient of electron emission $\delta = f(U_0)$. This mechanism can however be avoided by imaging at lower acceleration voltages, where at the worst positive charging can occur, which is a self-minimizing effect [13].

The second effect is due to high contact resistance $R_{contact}$ between part and ground. This has to be taken into account for parts which are consumed during the assembly cycle. There, the mechanical connection is kept loose in order to allow for easy picking of the parts in the handling sub-process. For estimating the charging of a part, it will be modeled as capacitor and an ohmic resistor, which are charged by the e-beam with the current I_P. This leads to a surface voltage U_S, cp. Fig. 5.

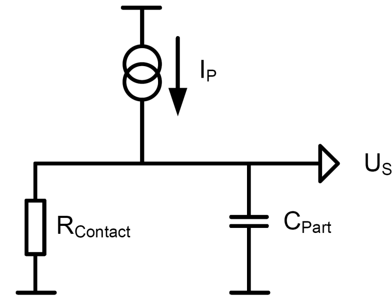

Fig. 5. Model used for estimating the surface voltage U_S which builds up during scanning a part with ohmic contact resistance $R_{Contact}$ and capacitance C_{Part} by an electron beam with current I_P.

This time-variant surface charge $U_S(t)$ can then be calculated by:

$$U_S(t) = I_P \times R \times (1 - e^{-\frac{t}{R_{Contact} \times C_{Part}}}), \quad (3)$$

where the capacitance of the part can be estimated from maximum surface charge ($26.5\,\mu\text{C/m}^2$). Assuming a contact resistance of 10 $M\Omega$ and a probe current of 1 μA pointed towards a dielectric object with $10\mu m$ in diameter, a voltage of $U_S = 10\,\text{V}$ will be build up after $0.6\,\mu$s. This charge results in major disturbances of the whole system: At first, due to the electrostatic forces, parts which are charged similarly, can move around if they overcome i.e. adhesive surface forces. Secondly, the charging has a major influence on the SEM-image. Typical effects here are image drift (deflection of primary electron beam), local changes in brightness and contrast and even artifacts like image distortion can occur. The time variant behavior of charging (and discharging) depends on major SEM-parameters like beam current, voltage and image scan time and thus results in hardly controllable effects.

C. Substrate Surface Modification Through E-Beam Interaction

When the primary electron beam hits the substrate, e.g. the tool, part carrier or part, the energy of the beam is dissipated by several physical effects. While the effect of substrate heating can be mostly neglected [13], [14], electron–substrate interaction can trigger chemical reactions between the residual gas-atmosphere in the vacuum chamber and the substrate surface. Although it is known from electron beam induced etching (EBiE) experiments on silicon substrates, that the

SEM's electron beam can dissociate the covering silicon oxide layer [15], [16], [17], the influence of this mechanism can be considered low on imaging artifacts.

Instead it is known since the early days of electron beam – substrate interactions, that residuals in the vacuum chamber form thin contamination layers on the substrates. R.L. Stewart is the first known to investigate this effect referred to as contamination deposition [18]. In his research, he found out that mainly organic vapors are dissociated and form (insulating) carbonaceous films on the substrate surface. Since the 1950s, this effect still is under investigation and since 20 years it is used for nano-scale deposition in the SEM (overview in [19]). Further applications include the assembly within the SEM (overview in [14]).

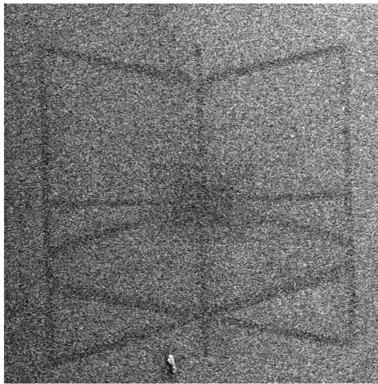

Fig. 6. E-Beam interaction induced contamination of a silicon substrate. The dark tracks are carbon contaminations during regular actuator movements in a scanning process. The scan field width is $27.2\,\mu$m.

On silicon substrates, the dissociation of hydro-carbons from the residual atmosphere in the vacuum chamber leads to the deposition of carbonaceous layers on the silicon. However, this layer changes the SE emission characteristics leaving the substrate (cp. Fig. 6). The common escape depths for SE is considered 30 nm [13] due to their low energy below 50 eV. With growing deposition layer thickness, the emission characteristic changes from that of silicon to that of carbon, i.e. the SE-yield δ changes from 0.30 for silicon [20] to 0.28 for carbon [20] at an acceleration voltage of 20 keV. Consequently, the number of emitted SE decreases while the contamination layer is deposited and thus the image brightness is reduced.

Typical sources for hydro-carbons in the atmosphere of the vacuum chamber are back-diffused pump oils from e.g. rotary pumps [21], [22], gaskets and o-rings and naturally organic residuals on any surface in the vacuum chamber [21], e.g. residuals from cleaning. Depending on the concentration of residuals in the vacuum chamber, deposition rates in the range of several nanometers per minute have to be considered [22], [23].

Typical countermeasures for reducing the contamination deposition are oil-free vacuum pumps and the fixture of cold traps to prevent back-diffusion into the vacuum chamber. The vacuum chamber itself and if possible the build-in parts can be cleaned with plasma cleaners in order to reduce the amount of adsorbed hydro-carbons on the vacuum chamber walls. However, during the assembly process EBiD or EBiE are applied to mount or to separate parts respectively. For this purpose, gas injection systems are fitted to allow for defined injection of process gases. This results in adsorption of potentially contaminating species on the surfaces and elongated idle time between gas assisted processing and imaging to prevent contamination deposition.

TABLE III

ALIGNMENT SEQUENCE COMMAND STATISTIC OF A CANTILEVER AND A CARBON NANOTUBE. GOAL OF THE SEQUENCE IS TO HORIZONTALLY ALIGN BOTH PARTS WITH A RELATIVE DISTANCE OF 300 NM.

Process primitives	Number of commands	Proportion
auto-focus	512	46.63%
auto-bc	394	35.88%
find position	31	2.82%
movement	32	2.91%
support functions	129	11.75%
sum	1098	

D. Results E-Beam Interaction

The different sources of disturbances on the assembly system are reflected in the commands of an automation sequences. For test purposes an alignment sequence has been developed. The purpose of this sequence is to align a fine etched metal tip (STM-tip) with a carbon nanotube (CNT). The CNT is positioned on the SEM-stage, while the STM-tip is fixated on the c-stage (cp. Sec. II). The alignment sequence is finished as soon as the relative distance of both parts is below 300 nm. The goal is achieved by iterative zoom and center steps. For every magnification level (150x, 800x, 4000x) the CNT and the cantilever is centered before switching into the next magnification level. The initial positions have been taught-in such that both objects are in the field of view of the SEM at a magnification level of 25x. During the whole procedure the CNT is positioned on the left part of the SEM image, while the cantilever is kept on the right part. This reduces the possibility of a collision.

The automation sequence has been executed (see Fig. 7) and the output of the sequence has been logged. The result can be found in Tab. III. The process primitives are grouped into auto-focus, auto-bc, find position, movement and support functions. Auto-focus process primitives are required to determine the working distance of the objects, auto-bc commands keep the contrast and brightness values inside an acceptable limit such that reliable visual servoing results can be achieved. "Find position" commands return the visual servoing feedback and movement commands include all SEM-stage and c-stage movements. Finally support functions consist of all functions not belonging to any other category such as "adjust sampling rate" and "switch magnification" process primitives. The relative high number of image optimization commands of 82.51% in contrast to 5.73% find position and movement commands is quite typical for SEM assembly sequences and due to the intrinsic and e-beam interaction based effects illustrated in this paper.

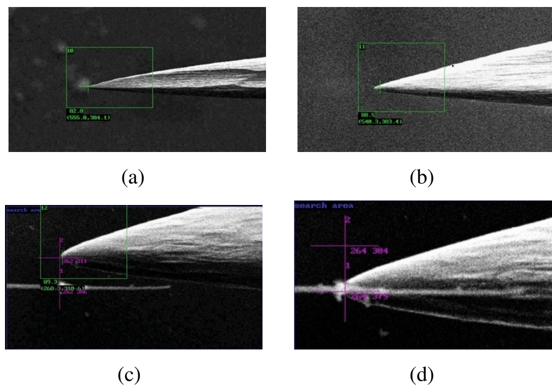

Fig. 7. SEM images of the alignment process at different scan field widths (sfw): (1) STM-tip above the CNT substrate (sfw 1.15 mm), (b) centered STM-tip (sfw 201.52 μm), (c) STM-tip and CNT aligned in x and z (sfw 39.936 μm), (d) Goal position: x, y and z aligned (swf 39.936 μm).

The number of auto-focus process primitives can be traced back to two facts. The z-Information is quite limited inside the SEM. Therefore, the focus depth is required for a rough estimation of the z position of objects. Secondly, the misalignment between vision and actuator coordinate system leads to z displacements, while moving in the x, y plane of the actuator. The low depth of focus of the SEM, which is in the scale of the scan field, lowers this influence for smaller magnification levels. For movements inside the current field of view of the SEM this effect is negligible unless the relative distance exceeds half of the scan field size.

The number of auto-bc process primitives is mainly due to e-beam interaction based disturbances. In the beginning of the sequence the STM-tip is moved into the field of view and the contrast and brightness values are adjusted. This is required to enable visual servoing and precise positioning of the STM-tip. In the second step the CNT substrate is moved below the STM-tip. This results in shading of the SEM image (cp. Par. IV-A). This needs to be compensated in order to enable CNT position tracking. During the zoom and center steps additional auto-bc steps are required. This is due to substrate surface modifications (cp. Fig. 6), which need to be compensated too.

V. CONCLUSION AND FUTURE WORK

This paper investigated different disturbance sources on a nano-assembly system inside the SEM. The influence of thermal drift has been simulated and actuator sensor alignment and end effector vibrations have been experimentally quantified. Electron-beam interactions, such as shading, charging effects and substrate surface modification through e-beam interaction have been modeled. The impact of shading and e-beam surface modifications on an example automation sequence has been analyzed. While effects such as charging and thermal drift can be reduced by appropriate grounding and minimizing thermal power loss, some need to be addressed during the development of appropriate automation sequences (e.g. mechanical vibrations, shading, etc.). This will lead to a major improvement in assembly cycle times and reliability. The influence of extrinsic sources, such as acoustic noise and building vibrations will be studied in the future.

REFERENCES

[1] E. K. Eigler, D. M.; Schweizer, “Positioning single atoms with a scanning tunnelling microscope,” *Nature*, no. 344, pp. 524 – 526, 1990.

[2] K. N. Mitsuishi, M.; Kobayashi, “Development of tele-operated micro-handling/machining system based on information transformation,” *Proceedings of the 1993 IEEE/RSJ International Conference on Intelligent Robots and Systems ’93, IROS ’93*, 1993.

[3] Y. Morishita, H.; Hatamura, “Development of ultra-micromanipulator system under stereo SEM observation,” *Proceedings of the 1993 IEEE/RSJ International Conference on Intelligent Robots and Systems ’93, IROS ’93*, 1993.

[4] T. S. Miyazaki, H.; Kameya, “Construction of an ultra-micro manipulation system based on visual control -realization of nano-hand-eye system,” *Proc. IEEE Symposium on Emerging Technologies and Factory Automation, 1994. ETFA ’94*, 1994.

[5] T. Wich and H. Hülsen, *Automated Nanohandling by Microrobots*. Springer Verlag, 2008, ch. Robot-based Automated Nanohandling.

[6] S. Fatikow, T. Wich, H. Hlsen, T. Sievers, and M. Jhnisch, “Microrobot system for automatic nanohandling inside a scanning electron microscope,” *IEEE-ASME Transactions on Mechatronics*, 2007.

[7] T. Sievers, “Global sensor feedback for automatic nanohandling inside a scanning electron microscope,” in *Proc. Virtual Int. Conference on Intelligent Production Machines and Systems (IPROMS’06)*, July 2006, pp. 289–294, http://conference.iproms.org/.

[8] B. Vikramaditya and B. Nelson, “Visually guided microassembly using optical microscopes and active vision techniques,” *Proceeding of the 1997 IEEE International Conference on Robotics and Automation*, 1997.

[9] S. Fatikow, J. Seyfried, S. Fahlbusch, A. Buerkle, and F. Schmoeckel, “A Flexible Microrobot-Based Microassembly Station,” *Journal of Intelligent and Robotic Systems*, vol. 27, no. 1-2, pp. 135–169, 2000.

[10] Numerik Jena GmbH Germany, “Datenblatt der positionssensoren l4,” 2008.

[11] T. Sievers, “Global sensor feedback for automatic nanohandling inside a scanning electron microscope,” in *Proceedings of IPROMS NoE Virtual International Conference on Intelligent Production Machines and Systems*, 2006, pp. 289–294, received the Best Presentation Award.

[12] B. E. Kratochvil, “Visual tracking for nanorobotic manipulation and 3d reconstruction in an electron microscope,” Ph.D. dissertation, ETH Zurich, 2008.

[13] L. Reimer, *Scanning Electron Microscopy – Physics of Image Formation and Microanalysis*, 2nd ed., ser. Springer Series in Optical Sciences, H. K. V. Lotsch, Ed., 1998, vol. 45.

[14] T. Wich, *Automated Nanohandling by Microrobots*. Springer Verlag, 2008, ch. Nanostructuring and Nanobonding by EBiD.

[15] S. Thomas, “Electron-irradiation effect in the auger analysis of sio2,” *Journal of Applied Physics*, vol. 45, no. 1, pp. 161–166, 1974.

[16] B. Carriere and B. Lang, “A study of the charging and dissociation of sio2 surfaces by aes,” *Surface Science*, vol. 64, pp. 209–223, 1977.

[17] S. J. Randolph, J. D. Fowlkes, and P. D. Rack, “Effects of heat generation during electron-beam-induced deposition of nanostructures,” *Journal of Applied Physics*, vol. 97, no. 12, p. 124312, 2005.

[18] R. L. Stewart, “Insulating films formed under electron and ion bombardment,” *Phys. Rev.*, vol. 45, no. 7, pp. 488–490, Apr 1934.

[19] I. Utke, P. Hoffmann, and J. Melngailis, “Gas-assisted focused electron and ion beam processing and fabrication,” *J. Va. Sc. Technol. B*, vol. 26, no. 4, pp. 1197–1276, 2008.

[20] H. Seiler, “Secondary electron emission in the scanning electron microscope,” *Journal of Applied Physics*, vol. 54, no. 11, pp. R1–R18, 1983.

[21] A. E. Ennos, “The sources of electron-induced contamination in kinetic vacuum systems,” *British Journal of Applied Physics*, vol. 5, no. 1, pp. 27–31, 1954. [Online]. Available: http://stacks.iop.org/0508-3443/5/27

[22] R. W. Christy, “Formation of thin polymer films by electron bombardment,” *Journal of Applied Physics*, vol. 31, no. 9, pp. 1680–1683, 1960. [Online]. Available: http://link.aip.org/link/?JAP/31/1680/1

[23] J. Ling, “An approximate expression for the growth rate of surface contamination on electron microscope specimens,” *British Journal of Applied Physics*, vol. 17, no. 4, pp. 565–568, 1966. [Online]. Available: http://stacks.iop.org/0508-3443/17/565